Geofísica Internacional (2026) **65-2**: 1- 23

Impact Assessment of Flood Extent on Agricultural Land and Communities Using Google Earth Engine and SAR Data: A Case Study of Indus River Basin

Ayesha Hassan[1], Muhammad Ismail Khan[2,3]*, Nisar Ali Shah[2,3], Mark E. J. Cutler[1]

Abstract

The Indus River Basin has undergone significant hydrological changes due to climate change, leading to increased flood frequency, posing a risk to agriculture-based food security. This study focused on rain-induced flood events from August to September 2022 across the provinces of Punjab, Sindh, and Baluchistan using Google Earth Engine, Sentinel-1A Synthetic Aperture Radar (SAR) data, and Landcover datasets. Flooding caused considerable damage to agricultural land and communities, affecting 49,602.92 km^2 of land. In Sindh, the total land inundated is 2,042.1 km^2 with 915.9 km^2 of agricultural land and 609.8 km^2 of built-up areas affected. Hence, district-level damage assessment includes Sukkur (497.1 km^2), Sanghar (565.2 km^2), and Khairpur (979.9 km^2). In Baluchistan province, the flooded area was 10,733.4 km^2. The agricultural land affected was 674.8 km^2, and 47.8 km^2 of built-up land. Heavy rain further intensified flooding affected 1002.2 km^2 in Jhal Magsi, 7,266.5 km^2 in Khuzdar, and 2,464.7 km^2 in Lasbella. In Punjab, 4001.3 km^2 of land flooded including 297.6 km^2 of built-up areas, and 776.9 km^2 affected agricultural land. At the District-level affected areas were D.G. Khan (1,871.3 km^2), Muzaffargarh (620 km^2), and Rajanpur (1,509.7 km^2). integration of remote sensing and GEE provided crucial flood insights and climate risk reduction strategies, especially in data-scarce regions.

Key words: Climate change, Flooding events, SAR, Google Earth Engine, Remote sensing, LULC, Pakistan.

Resumen

La Cuenca del Río Indo ha experimentado cambios hidrológicos significativos debido al cambio climático, lo que ha llevado a un aumento en la frecuencia de inundaciones, representando un riesgo para la seguridad alimentaria basada en la agricultura. Este estudio se centró en eventos de inundación inducidos por la lluvia desde agosto hasta septiembre de 2022 a través de las provincias de Punjab, Sindh y Baluchistan utilizando Google Earth Engine, datos de Radar de Apertura Sintética (SAR) Sentinel-1A y conjuntos de datos de Cobertura del Suelo. Las inundaciones causaron daños considerables a las tierras agrícolas y a las comunidades, afectando 49,602.92 km^2 de tierra. En Sindh, el total de tierra inundada es 2,042.1 km^2 con 915.9 km^2 de tierra agrícola y 609.8 km^2 de áreas construidas afectadas. Por lo tanto, la evaluación de daños a nivel distrital incluye Sukkur (497.1 km^2), Sanghar (565.2 km^2) y Khairpur (979.9 km^2). En la provincia de Baluchistan, el área inundada fue 10,733.4 km^2. La tierra agrícola afectada fue 674.8 km^2, y 47.8 km^2 de terrenos construidos. La lluvia intensa extendió aún más las inundaciones afectando 1002.2 km^2 en Jhal Magsi, 7,266.5 km^2 en Khuzdar y 2,464.7 km^2 en Lasbella. En Punjab, 4001.3 km^2 de tierra se inundaron incluyendo 297.6 km^2 de áreas construidas, y 776.9 km^2 afectaron tierra agrícola. A nivel distrital las áreas afectadas fueron D.G. Khan (1,871.3 km^2), Muzaffargarh (620 km^2) y Rajanpur (1,509.7 km^2). La integración de la teledetección y GEE proporcionó información crucial sobre inundaciones y estrategias de reducción del riesgo climático, especialmente en regiones con escasez de datos.

Palabras clave: Cambio climático, Eventos de inundación, SAR, Google Earth Engine, Teledetección, LULC, Pakistan.

Received: August 2, 2025; Accepted: January 1, 2026; Published on-line: April 1, 2026.

Editorial responsibility: Mtro. Miguel Moctezuma-Flores

* Corresponding author: Muhammad Ismail Khan, muhammad_ismail@uop.edu.pk
[1] University of Dundee, School of Humanities, Social Sciences and Law, Dundee, United Kingdom.
[2] University of Peshawar, National Centre of Excellence in Geology, Khyber Pakhtunkhwa, Pakistan.
[3] National Centre of GIS and Space Applications, GIS and Space Application in Geosciences, Islamabad, Pakistan.

Ayesha Hassan, Muhammad Ismail Khan, Nisar Ali shah, Mark E. J. Cutler

https://doi.org/10.22201/igeof.2954436xe.2026.65.2.1907

1. Introduction

Natural disaster frequency and intensity have increased due to mechanisms resulting from climate change over the last few decades (Ahmad *et al.*, 2023; Zhao *et al.*, 2021). Climate change is increasing the frequency and intensity of rainfall, resulting in increasingly frequent and severe flooding occurrences (Khan *et al.*, 2021). Globally, communities are facing high economic and social losses as the frequency, severity, and distribution patterns of such natural calamities increased (Chan *et al.*, 2019). Flood disasters are the leading cause of human mortality and, more typically, social, and economic problems (Dube *et al.*, 2021; Ejeta, 2018). Therefore, this study focused on rain-induced flood occurrence in August to September 2022 in the Indus River which caused considerable damage to agricultural land and communities. Hence, remote sensing, Google Earth Engine (GEE) and Synthetic Aperture Radar (SAR) approaches can play a key role in making well-informed spatial planning decisions and developing disaster risk reduction policies (Mbah *et al.*, 2022).

Pakistan is considered the most sensitive country in the South Asian region to climate change due to inadequate natural resource management and crucial geographical locations (Ali *et al.*, 2017). Pakistan listed as the world's 29th most vulnerable state in 2009-2010, 16th in 2010-2011, and 5th highly susceptible country as of right now (Ali *et al.*, 2017). From 1950 to 2014, Pakistan experienced floods, including mild and severe flooding events (Manzoor *et al.*, 2022). Furthermore, from 2010 to 2014, Pakistan experienced a series of flood disasters, with the 2010 flood displacing nearly 20 million people, damaging 1.5 million homes, killing 1985 people, and destroying cropped and residential areas covering 160,000 km^2 (Qamer *et al.*, 2023). These disasters lowered animal, fiber, and food productivity (Asim *et al.*, 2021). They also made farming communities more vulnerable to threats to their livelihood and food shortages for those who depend on agriculture for their survival. Developing countries are more vulnerable to the effects of severe flooding events because they receive insufficient funding for adaptation and mitigation measures (Fankhauser and McDermott, 2014). In Pakistan flooding is a complicated problem with several causes and effects. Most often, Pakistan experiences floods in the main Indus River System because of irregular weather during the monsoon season and snowmelt, demonstrating that both pluvial and fluvial floods can happen (Shah *et al.*, 2023; Tariq *et al.*, 2020). Fluvial flooding caused by rising river water levels, whereas pluvial flooding caused by increased rainfall intensity (Try *et al.*, 2020). Due to extremely heavy monsoon rains in August 2022, Pakistan experienced one of its worst floods in recorded history (Ting, Biasutti and You, 2023). Since Pakistan came into existence, there has not been a major flood until eight years or so (Kirsch *et al.*, 2012). This is largely because of the intense monsoon rains in July and August, which caused significant losses to the economy, agriculture, infrastructure, and property. The 2010 floods damaged around 900,000 households and submerged an area of more than 70,000 km^2 (Haque *et al.*, 2012). In 2022, 33 million people affected by the most recent floods in Pakistan, which killed close to 1,739 people and destroyed vital infrastructure, agricultural land, and homes. According to P Lama and Tatu (2022), rainfall in Sindh was 726% above normal while in Balochistan it was 590%. The usual August rainfall for these provinces is 31 mm for Balochistan and 26 mm for Sindh, as per the Pakistan Meteorological Department (PMD's) baseline climatology. According to the World Weather Attribution Organization, the Pakistan Indus River Basin witnessed a 75% increase in intense precipitation during the preceding 60 days (Otto *et al.*, 2023). 2011 floods submerged more than 21,000 km^2 of land, forcing 5.9 million people to flee their homes, and more than 16,000 km^2 of agricultural land, 500 km^2 of forest, 382 km of rail tracks, and 1,500km of roads were destroyed (Haque *et al.*, 2012). Remote sensing is a significant source of spatial data in the event of a natural disaster, and its usefulness has been demonstrated on numerous occasions all over the world. However, there are various kinds of risks that occur annually throughout the world, and their remote sensing remedies are just as diverse (Joyce *et al.*, 2009). Effective flood risk management plans assist impacted communities and scientific knowledge by analyzing the range and impact of floods (Hoang *et al.*, 2018; Wang *et al.*, 2022). Furthermore, this study explores the impact of the floods that occurred in Pakistan in 2022 by utilizing Google Earth Engine and remote sensing capabilities. Through careful analysis of Sentinel-1 and Sentinel-2 satellite data, we have produced accurate maps of the pre-post flood dynamics, land cover, and flood extent. Our study aims to map pre-flood and post-flood inundations using Google Earth Engine and Sentinel-1, facilitating the identification of flooded areas and damage assessment. To better understand the impact of the flood on communities and agricultural/crop areas, we have carefully examined Sentinel-2 data to identify and measure changes in land use and land cover. The flooding in both agricultural fields and urban areas caused by exceptionally high monsoon rainfall, which was far above the long-term average, combined with inadequate drainage infrastructure, poor urban planning, and the overflow of rivers and canals. These factors contributed to a rapid rise in rainwater levels and extensive inundation. Our goal is to make a significant contribution to flood monitoring and management through this comprehensive research, guiding data-driven decision making for disaster risk reduction and sustainable development.

2. Materials and Methods

2.1. Description of Study Area

The research was conducted in District Sukkar, Khairpur, Sanghar, Jhal Magsi, Khuzdar, Lasbella, Rajanpur, DG Khan, and Muzaffargarh. The selected districts are in the center of Sindh, Baluchistan and Punjab provinces (Figure 1), which are major contributors to the agricultural production of the country and are particularly susceptible to flooding during the monsoon season. The study area stretches between 31.3369° N and 24.8998° N latitudes, and longitudinally from 71.7056° E to 65.6061° E. It shares its northern border with Dera Ismail Khan, eastern border with the districts of Multan and Khanewal, southern border with the Arabian Sea, and western border with the Washuk District. The region receives rainfall ranging from 28 mm to 140 mm, and the total agricultural land covers an area of 198,411.7 km^2.

The research area is located on the west shore of the Indus River Basin. The topography is remarkably diverse and is flat, characterized by the Indus River Delta plains, which makes it suitable for agricultural activities. Research areas also comprise rugged terrains, mountains, and plateaus and are a mix of coastal plains along the Arabian Sea. However, there is a risk of high flooding due to its proximity to the river system including, the Indus River which flows through Sukkur, Sanghar, Rajanpur, and DG Khan the Chenab River which flows through Muzaffargarh and the Porali River which flows near Khuzdar. An outsized proportion of the population inhabiting these areas relies heavily on agriculture as a means of subsistence. According to the 2017 census, the population of the current research area was 25,404,179. Satellite data is a valuable resource for understanding land evolution, particularly after floods allowing researchers to assess the extent to which the flooding has affected human settlements and agricultural productivity (Schumann *et al.*, 2022).

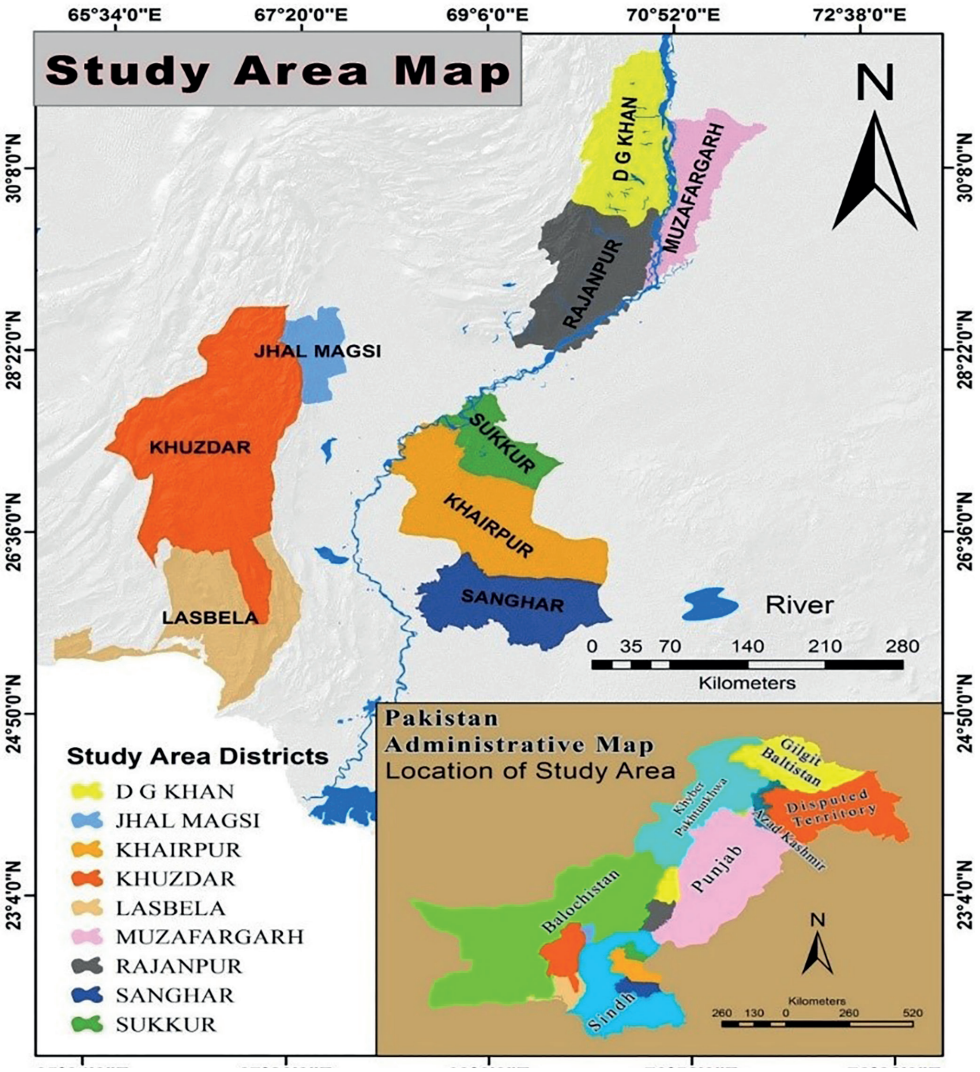


Figure 1. Map displaying the locations of the study regions, Sindh, Punjab, Baluchistan Province, Indus River

2.2. Data Used

Sentinel-1 SAR data used for flood inundation mapping. The flood damage assessment has been performed using Land Use Land Cover (LULC). The detailed data used, as well as the sensor characteristics, are given in Table 1. Cropland and built-up areas were extracted from the Sentinel-2 Copernicus Global Land Cover dataset, which was acquired from the European Space Agency (ESA). Sentinel-2 shortwave infrared (SWIR) bands were used in addition to conventional indices because they are extremely sensitive to clay minerals, which show prominent absorption characteristics in this spectral range. Due to its sensitivity to changes in surface mineral composition, multispectral imaging (RGB: VV, VH, and VV–VH in decibel units or VV/VH in linear units) can distinguish between soil and flood-affected areas both pre and post flood occurrences. By comparing the sensor's spectral signatures with known reference signatures of different minerals, algorithms and spectral analysis were used to find reflectance patterns linked to diverse clay kinds. To facilitate flood detection, several indices were computed, including the Normalized Difference Vegetation Index (NDVI), Normalized Difference Built-up Index (NDBI), Normalized Difference Water Index (NDWI). Although there are several water indices (such as MNDWI, AWEI, and WRI), NDWI was chosen because it is the most successful in differentiating open water bodies from vegetation and populated areas in this region's geography.

The agricultural area was extracted using ArcGIS 10.8 software. Shapefiles of the districts were used to get the flood impact area statistics at various levels. The Ground Range Detected (GRD) product of the Sentinel-1A satellite provided data in the C-band dual-polarization channels (VH and VV) with a repeat cycle of 12 days and was used to extract the flood-inundated area. The pixel spacing resolution of the Sentinel-1A data is 10 m. The SAR images were processed directly in GEE from August to September 2022 and used for identifying flood pixels.

2.3. Calculation Methods

NDVI was calculated in a raster calculator in ArcGIS following the equation for this index (Gao, 1996).

$$NDVI = \frac{(NIR-Red)}{(NIR+Red)} \quad (1)$$

NDBI was calculated in a raster calculator in ArcGIS following equation for this index (Zha *et al.*, 2003).

$$NDBI = \frac{(SWIR-NIR)}{(SWIR+NIR)} \quad (2)$$

NDWI was calculated in a raster calculator in ArcGIS following the equation for this index.

$$NDWI = \frac{(NIR-SWIR)}{(NIR+SWIR)} \quad (3)$$

2.4. Processing of Sentinel-1 SAR Data

According to the surface characteristics of the objects, like structure, humidity, texture, plant cover, etc., the backscattered signal (back scattering coefficient 0) is collected and amplified at specific frequencies and polarization modes by receivers in radar systems (Carreño and De Mata Muñoz, 2019). Radar pictures show a dual polarization of VV and VH intensity. Co-polarization (VV), which has a 0° phase difference between transmitted and received signals, is usually preferred over cross-polarization (VH), which has an evenly distributed phase difference between -180º and +180º and thus becomes less useful for mapping the water surface because it lacks target-specific information (Gan *et*

Table 1. Showing the data and source used in the current study.

Used Datasets	Spatial/ Temporal Resolution	Date of Acquisition	Determination	Data Source
Sentinel-1A (SAR)	10 m, 12 days	12th August-1st September (2022)	Flood extent mapping	ESA Copernicus Open Access hub
			Pre- and Post-Flood Images	
Sentinel 2A-2B (ESA)	10m	12th August-1st September (2022)	Pre- and Post-Flood NDWI	
			Pre- and Post-Flood NDVI	
	21 days		Pre- and Post-Flood NDBI	
			LULC classification/ Permanent water mapping	

In August and September 2022, flood inundations were further used to assess the damage caused by the floods across the agricultural areas and the urban regions.

al., 2012). Both VH and VV polarization were used, and it was discovered that while the flooded areas are overestimated by VH polarization, VV offers a more accurate representation (Clement *et al.*, 2017). Furthermore, choosing the same polarization (VV) for every image that is accessible provides superior outcomes for the subsequent interpretation process (Psomiadis *et al.*, 2020). Using the GEE, precise procedures were performed throughout the data preparation process for the radar images. After that, an image calibration was carried out, evaluating the measurement precision of the instrument against specific standards. A speckle filter was incorporated. Delineating the flooded region requires careful consideration when choosing a speckle filter. Speckle is a type of noise that reduces image quality and complicates interpretation. Therefore, before interpretation and analysis, it is frequently required to reduce the impact of the speckles (Rana and Suryanarayana, 2021). Several filter types and window sizes on the cloud GEE platform were used in the current investigation including Lee (3 × 3, 5 × 5 and 7 × 7), Lee Sigma (5 × 5, 7 × 7), Refined Lee and Gamma Map (3 × 3, 5 × 5 and 7 × 7). Sentinel-1A SAR data made publicly available by the European Space Agency (ESA) (sciHub: http://scihub.copernicus.eu) were used in this investigation. It has a receptivity frequency of 12 days for a single satellite and 6 consecutive days for two satellites. It is accessible in four modes, which are Strip Map (SM), Interferometric Wide swath (IW), Extra-Wide swath (EW) and Wave (WV). VH mode used in the study is the primary land surface acquisition mode that satisfies modern service requirements including continuing archives (Quintero *et al.*, 2012). All pre-processing tasks for SAR satellite data have been completed using the GEE platform.

2.5. Methodology

The main goal of the designed methodology was to offer a precise and accurate flood damage assessment for Pakistan's agricultural and urban areas through satellite imaging, as well as insightful analysis into practical flood inundation measures. The flood extent map was created using Sentinel-1A SAR data and a Change Detection (CD) approach, which involved comparing images taken before and during a flood. Pre-processing techniques including thermal noise reduction, radiometric calibration, terrain adjustment and speckle filtering were applied before map creation. Figure 2 depicts the detailed methodology of the current research work.

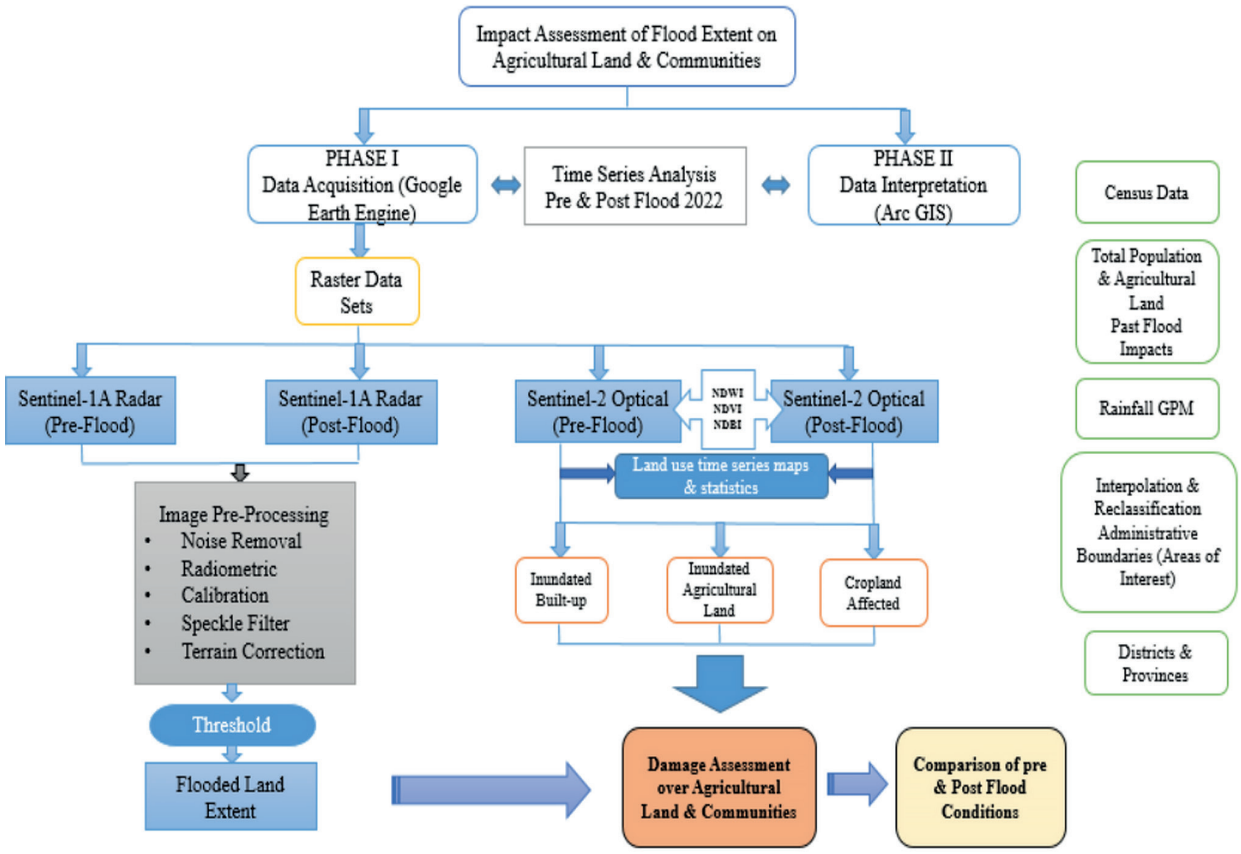


Figure 2. Flowchart illustrating the research work's methodology.

The geometric distortions present in SAR images were corrected through the application of terrain correction. The changes caused by flooding were computed by dividing the pre-flood mosaics by the during-flood mosaics using an upper limit of 1.52. brighter pixels with higher values in the final image displayed notable differences when compared to the more intense (low value) pixels. Subsequently with a threshold value of 1.52, a binary raster layer was formed, designating 1 for all values larger than 1.25 (flood pixels) and 0 for all values under 1.25 (non-flood pixels). The Copernicus Sentinel-2 data were utilized to extract the agricultural area for the full research region. To identify the agricultural land, LULC raster data was initially converted to a vector format. Then, classes containing identical values for the agricultural land were combined. Using the clipping tool, crop-covered pixels that merged with the extent of the flood inundation were determined to calculate the percentage of the cropland area affected by the total inundated area. The built-up area affected by flooding was extracted using the same technique. As indicated in Table 1, every Sentinel-1 SAR imagery that was available for mapping, monitoring, and flood-affected areas was used during the pre-flood period, which ran from August 12, 2022, to September 1, 2022.

3. Results

3.1 Rainfall Patterns During Floods

The August-September 2022 rainfall data for the provinces of Punjab, Sindh, and Baluchistan were examined to get a better understanding of hydro-meteorological factors that contributed to the 2022 flood event. With peak values ranging between 450 and 500 mm. The research shows that Sindh province received the most rainfall, especially in the districts of Khairpur, Sukkur, and Sanghar. While Punjab got between 200 and 300 mm of rainfall, mostly in the districts of DG Khan and Rajanpur, Baluchistan experienced between 300 and 400 mm, particularly in Jhal Magsi and Khuzdar (Khan *et al.*, 2021).

Baluchistan and lower Sindh had the highest concentration of precipitation. The substantial correlation between rainfall patterns and inundation severity is confirmed by the close correspondence among these zones and the flood hotspots found in the flood extent maps obtained from Sentinel-1 SAR. One of the main causes of the event's widespread flooding was the intense monsoon rains, worsened by upstream flooding.

3.2 NDVI, NDWI and NDBI-Time Series Maps of the Flood Extent

The Normalized Difference Vegetation Index (NDVI), Normalized Difference Built-up Index (NDBI) and Normalized Difference Water Index (NBWI) were mapped using the Copernicus Sentinel-2 data. The vegetation growth status is captured by the NDVI, the pixel's moisture content is reflected by the NDWI, and the built-up area is reflected by the NDBI.Three different time series from August to September were illustrated. To determine the extent of the areas affected by flooding in Punjab, Baluchistan, and Sindh provinces, the NDVI time series transformation was retrieved by using Sentinel-2 and it shows (Figure 4 and Figure 5) that August had the highest NDVI results. On the other hand, as Figure 3 illustrates, the flood caused an abrupt low point in the NDVI values for Sindh province. Therefore, the difference between pre and post-flood NDVI was used as an extraction feature.

The time series map of the NDWI for August-September 2022 was also extracted from the provinces of Sindh, Punjab, and Baluchistan using the same Sentinel-2 images. The NDWI value in 2022 is at its maximum value following the flood (Figures 6, 7 and 8). The time series change map for NDWI in August-September 2022 was created and shows the pre- and post-flood scenario. NDWI values are higher in the post-flood map. The flood extent was cross checked with the NDWI for validation to check whether the measured disaster extent is correctly mapped and depicts the same extent in the study area as the water index shown in Figures 6, 7 and 8.

The impact of flood inundation on built-up land is a critical issue for urban planning and disaster management. The flood extent overlay map depicted in Figure 9 shows the affected urban area estimated to be 10,576.1 km^2. Evaluating the potential effects of flooding on developed areas helps in decision-making, risk assessment, and mitigation strategies (Figures 9, 10, 11).

Overlaying the flood extent maps onto land use and building footprint data to assess the potential damage to built-up areas was performed.

The study provided insight into developing flood risk maps and hazard maps to guide urban planning and disaster management efforts. The NDVI, NDWI and NDBI indices are each sensitive to the growth of vegetation, soil humidity and infrastructure. They are all successfully incorporated into the present research approach to guarantee the efficacy of flood extent because they each play a significant role in the recognition of flood information.

3.3. Permanent Water Detection

Detecting permanent water bodies using SAR data and Sentinel-2 data is a common approach in remote sensing and earth observation (Bai *et al.*, 2021). SAR data can help detect water bodies even in challenging conditions like cloud cover or darkness. Sentinel-2 satellites provide optical and multispectral data,

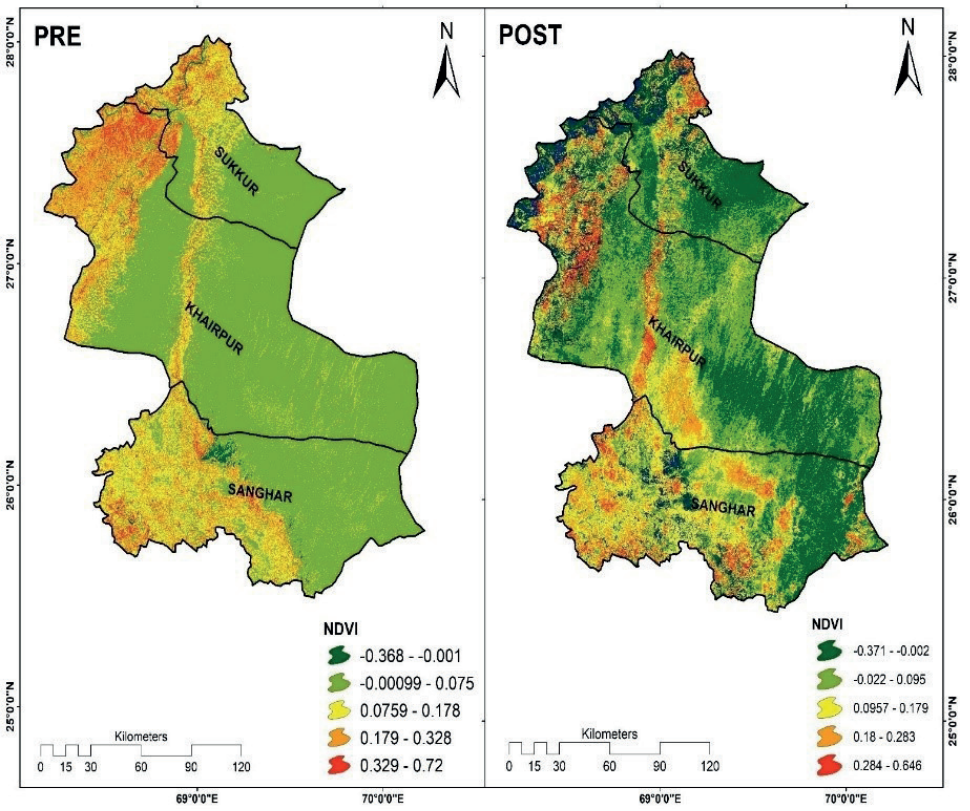


Figure 3. NDVI images represent the presence of vegetation and non-vegetation of Sindh Province, Pakistan.

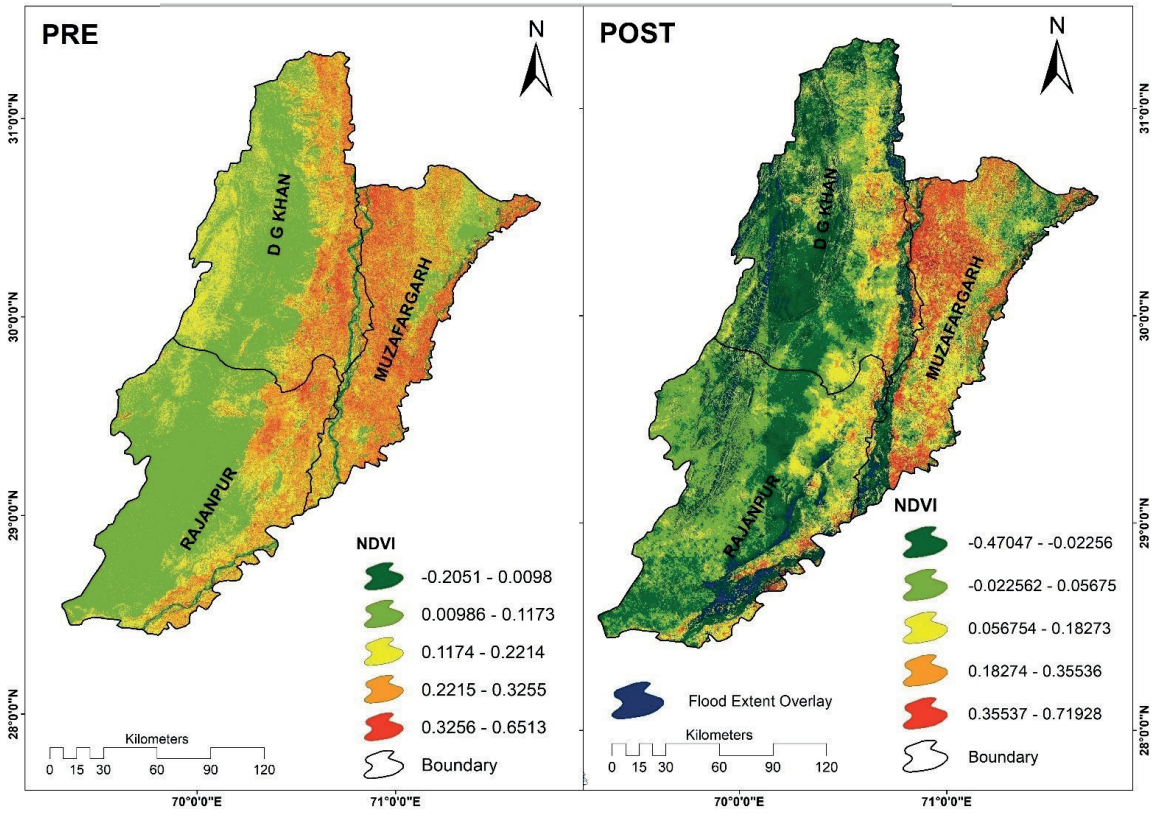


Figure 4. NDVI images representing the pre and post flood extent overlay in Punjab Province, Pakistan.

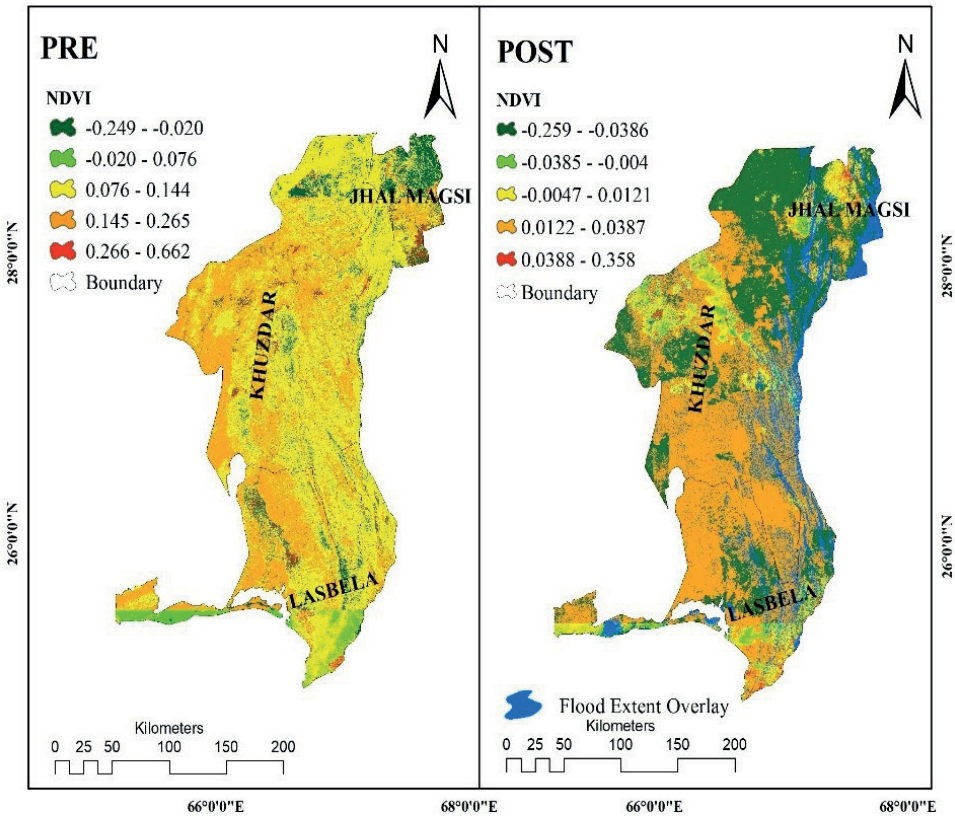


Figure 5. NDVI images representing the pre and post flood extent overlay in Baluchistan Province, Pakistan.

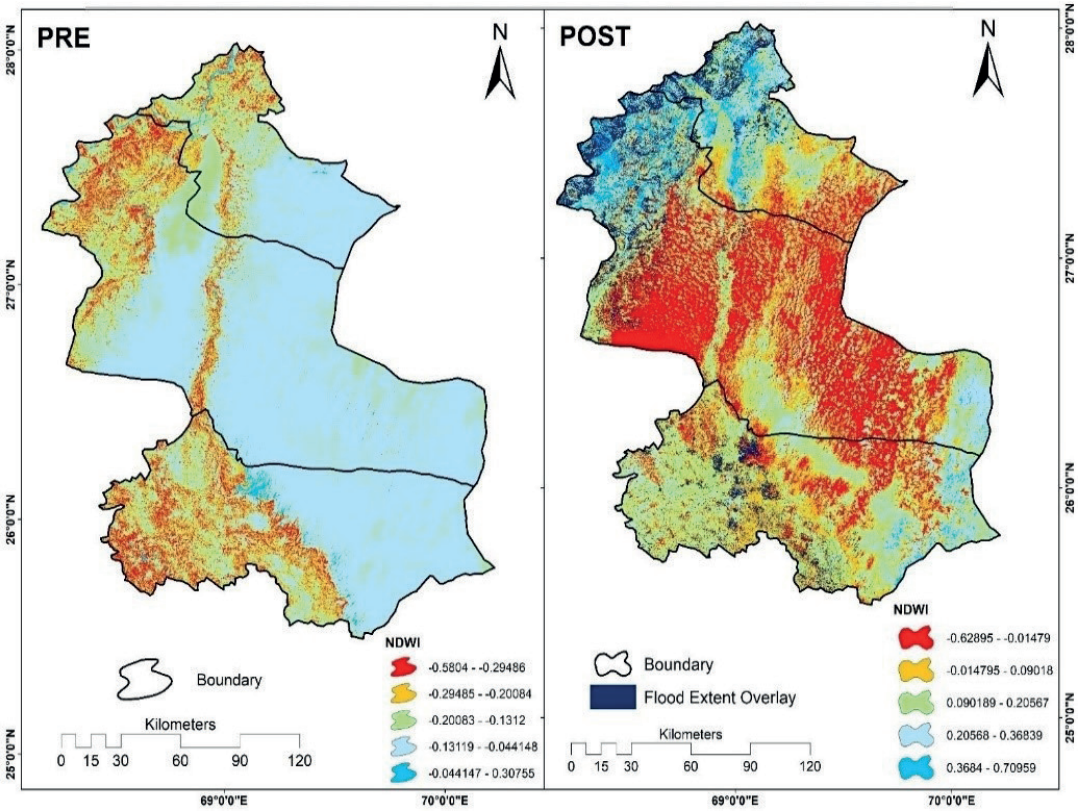


Figure 6. Map showing the pre and post flood extent overlay in NDWI of the Sindh Province, Pakistan.

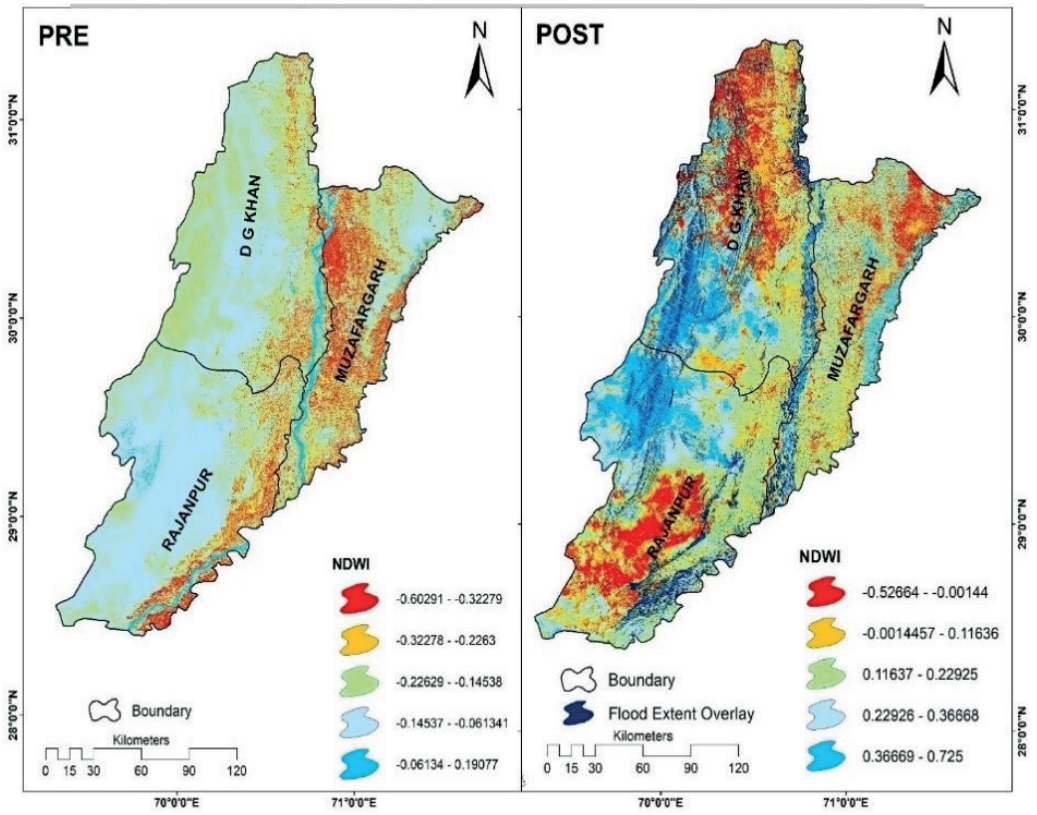


Figure 7. Map showing the pre and post flood extent overlay in NDWI of the Punjab Province, Pakistan.

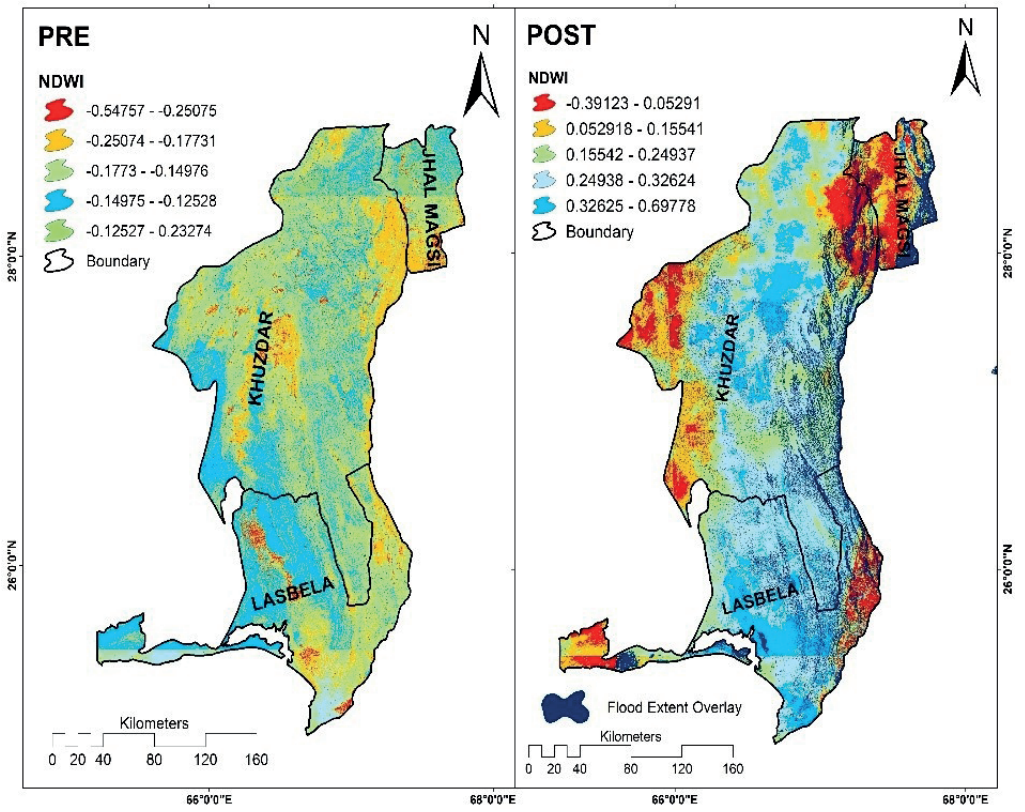


Figure 8. Map showing the pre and post flood extent overlay in NDWI of the Baluchistan Province, Pakistan.

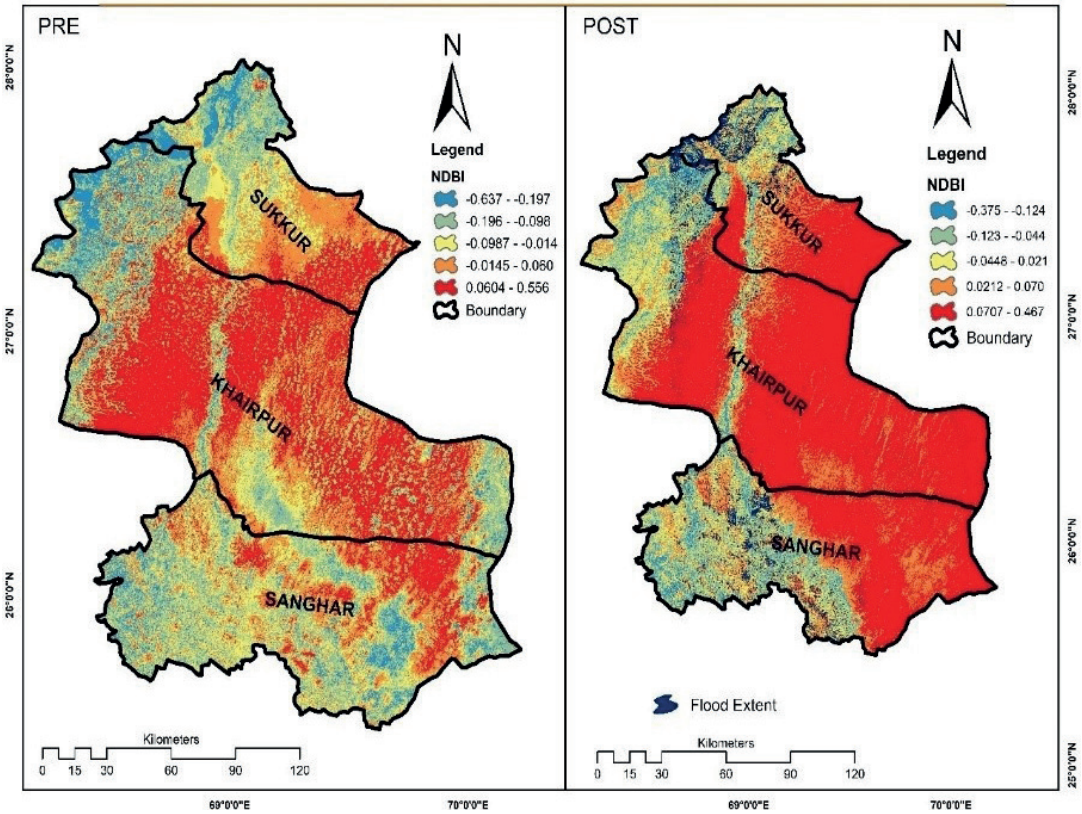


Figure 9. Map showing the pre and post flood extent overlay in NDBI of the Sindh Province, Pakistan.

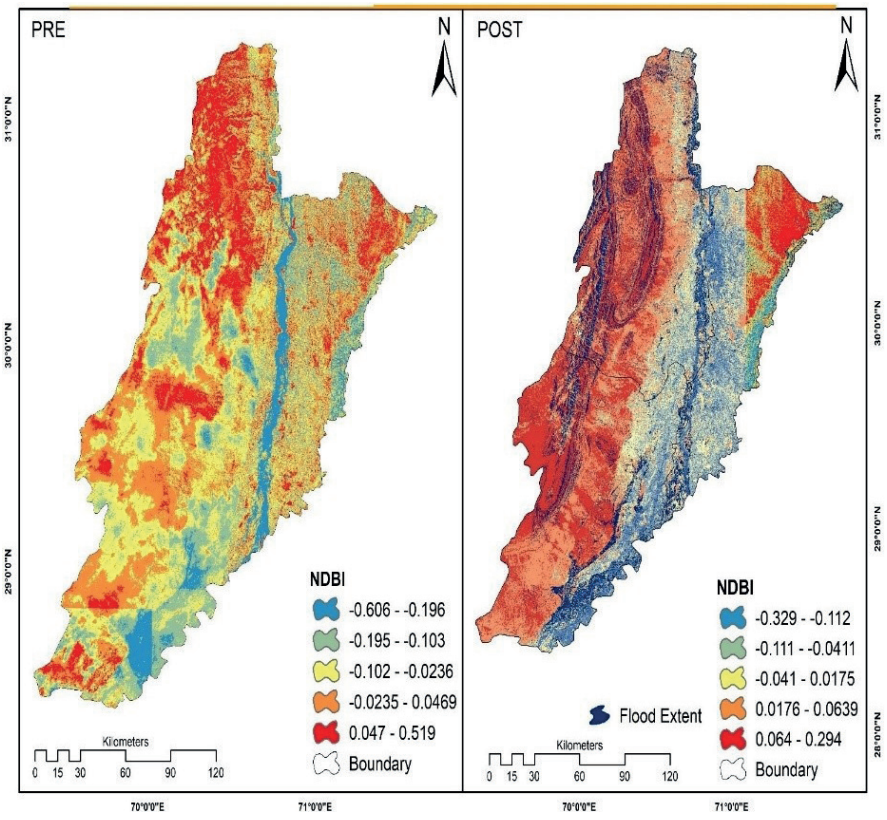


Figure 10. Map showing the pre and post flood extent overlay in NDBI of the Punjab Province, Pakistan.

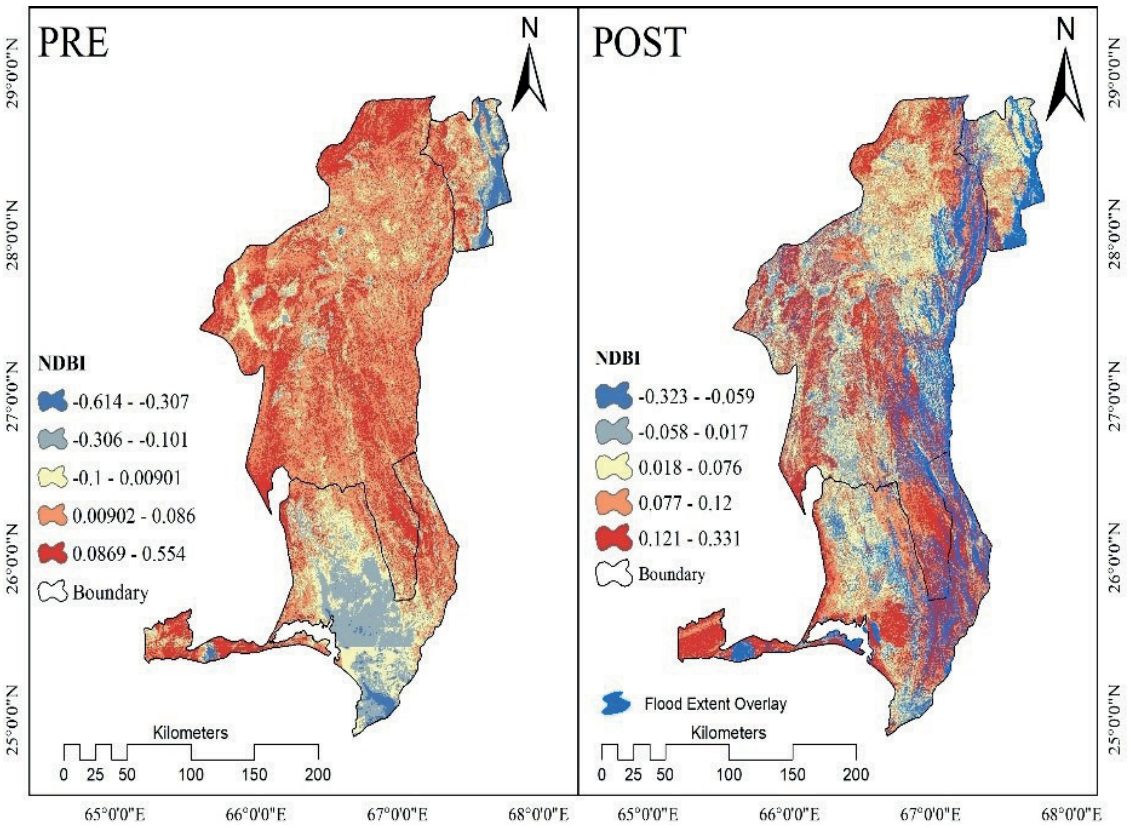


Figure 11. Map showing the pre and post flood extent overlay in NDBI of the Baluchistan Province, Pakistan.

capturing information in different spectral bands. These datasets can be accessed through platforms like the Copernicus Open Access Hub. Fuse the SAR and Sentinel-2 data to combine their strengths. This was performed by overlaying and combining their information to create a more comprehensive image. The spectral indices (like NDWI) were used to identify water bodies (Figures 6, 7 and 8). The estimated size of permanent water bodies was 17,947.18 km^2 (Table 5). The pre and post-comparison shows a relatively high degree of coherence between the two maps for each province, particularly around the river's coast.

3.4. Flood 2022 Impact on Agricultural Land

The impacted agricultural area and built-up land that have been affected by flooding were extracted using the Copernicus Sentinel-2 dataset with a 10 m spatial resolution for the selected provinces. Floods had negative effects on built-up and agricultural lands, affecting an estimated area of 49,602.9 km^2 and 10,576.1 km^2 of the study regions. Analysis shows that the inundated agricultural land in district Khairpur covered an area of 531.2 km^2, the Sanghar inundated area was 100.6 km^2 while Sukkur was flooded 284.2 km^2 from Sindh province (Table 2, Figure 12).

Study shows that inundated agricultural land in the district DG Khan covered an area of 131.3 km^2, while Muzaffargarh was 280.5 km^2 and Rajanpur district was flooded 364.22 km^2 (Table 3, Figure 13).

The inundated agricultural area for district Jhal Magsi was 417.2 km^2, the district Khuzdar flooded agricultural area is 102.3 km^2 and 155.2 km^2 was in district Lasbela (Table 4, Figure 14).

For agricultural region extraction, the Sentinel-2 dataset product was classified using the maximum likelihood supervised classification method, and the output image was used for agriculture area extraction purposes (Figure 15). The LULC raster data was initially transformed into a vector format, and classes with similar values for each cropland were combined to extract the crops and agricultural land. Additionally, a clipping tool was used to extract the cropland pixels that overlapped the degree of flood inundation to estimate the area of cropland and agricultural land affected by the total inundated flood (Figures 12-14).

The flooded built-up area was extracted using the same procedure. The spatial pattern illustrates the negative impact of the floods on the croplands. Tables 2-4 provides regional statistics of the built-up and agricultural areas damaged by the floods. The study area includes all agricultural land and built-up areas,

Table 2. Table showing the Inundated Agricultural Land and Built-Up Punjab Province.

Inundated Agricultural Land and Built-Up Province of Sindh	Area Affected		Area Affected	
	Built-Up		Agricultural Land	
	Km²	%	Km²	%
Khairpur	140.29	52.81	531.22	57.99
Sanghar	100.10	37.68	100.55	10.97
Sukkur	25.22	9.49	284.22	31.02
Total	265.61	100	915.99	100

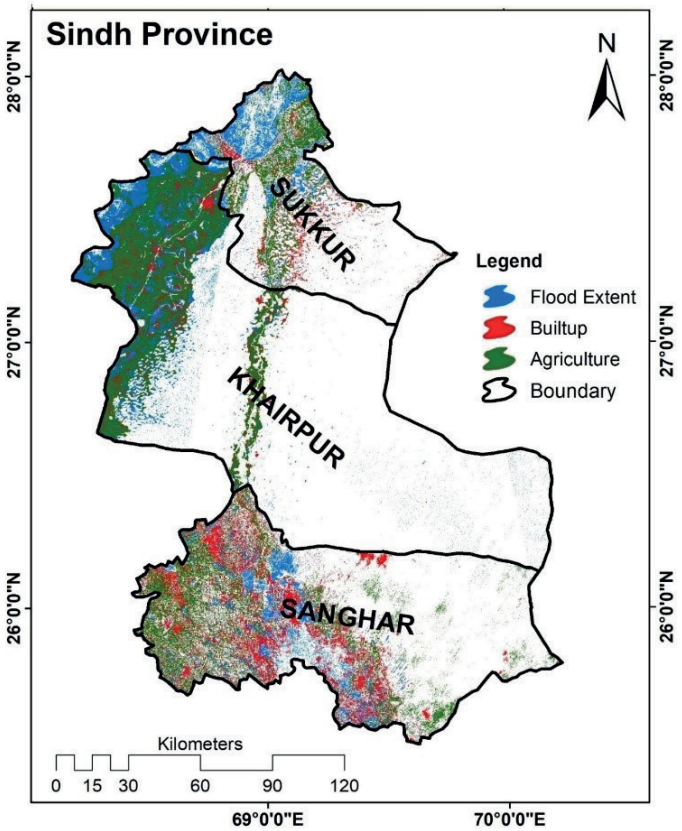


Figure 12. Map showing the flood-effected built-up area and Agricultural land of the Sindh Province, Pakistan.

accounting for 13.5% and 2.9% of the total land use and land cover, respectively. In 2022, flood events affected 2365.3 km² and 607.8 km² of farmland and built-up areas.

3.5. Land Use/Land Cover Classified Map

The present study used the maximum likelihood classification approach to determine the final pre and post-LULC maps for the provinces of Baluchistan, Sindh, and Punjab. The land cover classes were agricultural land, cropland, forest, rangeland, built-up areas, bare ground, snow, water, and cloud cover (Figures 15,16,17). Crop areas and agricultural land cover 13.5% (198,411.7 km²) and 0.05% (858.5 km²) of the basins, mainly in the mountainous regions, with crops primarily inhabiting the basin's center plain. The majority of the plain, or 14.4% (261.6 km²) of the basin, and 52.9% of all cultivated land, is taken up by summer crops. Winter crops are grown on the remaining agricultural land's barren soils (24.5%), forest land 2.5% (36,831.1 km²), built-up area 2.9% (42,304.3 km²), rangeland 55.3% (814,340.5 km²) and other land (25.5%) (Table 5).

The maps were created provincially to measure the land cover accurately. The dominant land cover classes for Baluchistan province were built-up with a total land area of 211 km², crops

Table 3. Table showing the Inundated Agricultural Land and Built-Up Baluchistan Province.

Inundated Agricultural Land and Built-Up Province of Punjab	Area Affected Built-Up		Area Affected Agricultural Land	
	Km²	%	Km²	%
DG Khan	30.47	30.47	131.33	16.92
Muzaffargarh	110.77	110.77	280.45	36.14
Rajanpur	156.33	156.33	364.22	46.93
Total	297.57	297.57	776	100

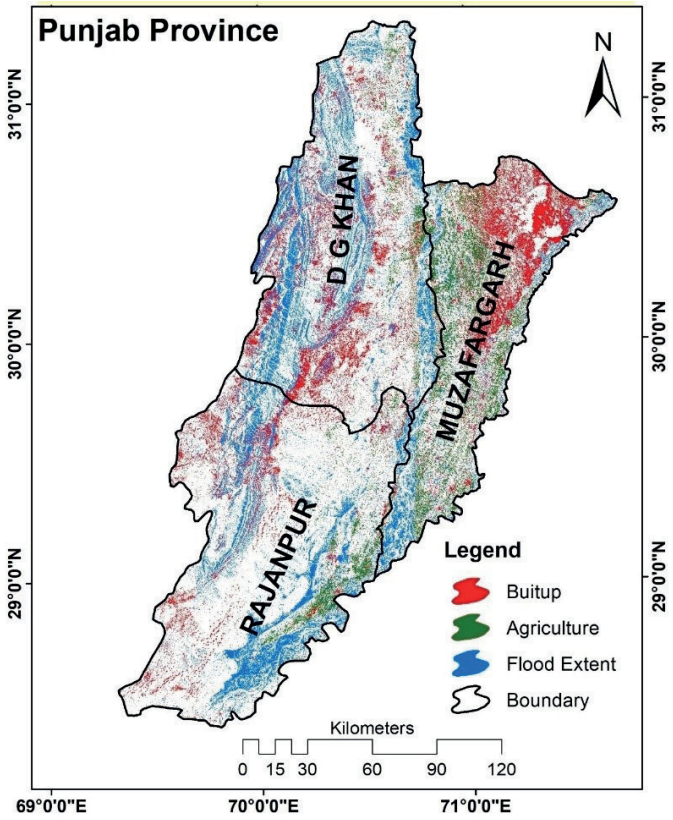


Figure 13. Map showing the flood-effected built-up area and Agricultural land of Punjab Province, Pakistan.

(2,231 km²), water bodies (145 km²), rangeland (40,346 km²), forest (2 km²), and bare ground (2,447 km²) (Table 6).

While the Punjab province built-up is covering an area of 1,752 km², crops (12,547.6 km²), water bodies (676.9 km²), rangeland (15,129 km²), forest (71 km²), bare ground (1,593 km²) and cloud cover (90 km²) (Tables 3 and 7).

The merging of Sentinel-1 and Sentinel-2 datasets allowed for coverage of the whole period between early August and early September while also resolving visibility issues brought on by dense cloud cover, especially when the water level first started to rise, on July 12 and September 1. Certainly, the Sentinel 1-2 image from the 31st of September enables one to infer from the few regions that are mostly covered by clouds, whereas the 1st of September depicts the initial inundation in the floodplain (Figure 15). Due to the proximity of the Indus River to Sindh, Baluchistan, and Punjab, it is expected that, in contrast to the exact time of the floods that hit the Khairpur, Sanghar, and Sukkur regions, the maximum inundation phase in the districts of DG Khan, Muzaffargarh and Rajanpur was delayed by approximately a week and continued for an additional 10 to 15 days. The peak inundation is temporarily constrained by the Sentinel-2 products on August 31 and September 1, and the Sentinel-1 image on August 31 and September 1. Sentinel-2 data from August 12 and the image from September 1 taken

Table 4. Table showing the Inundated Agricultural Land and Built-Up Punjab Province.

Inundated Agricultural Land and Built-Up Province of Baluchistan	Area Affected		Area Affected	
	Built-Up		Agricultural Land	
	Km²	%	Km²	%
Jhal Magsi	5.35	11.19	417.22	61.83
Khuzdar	10.22	21.38	102.33	15.16
Lasbela	32.22	67.41	155.22	23.00
Total	47.79	100	674.77	100

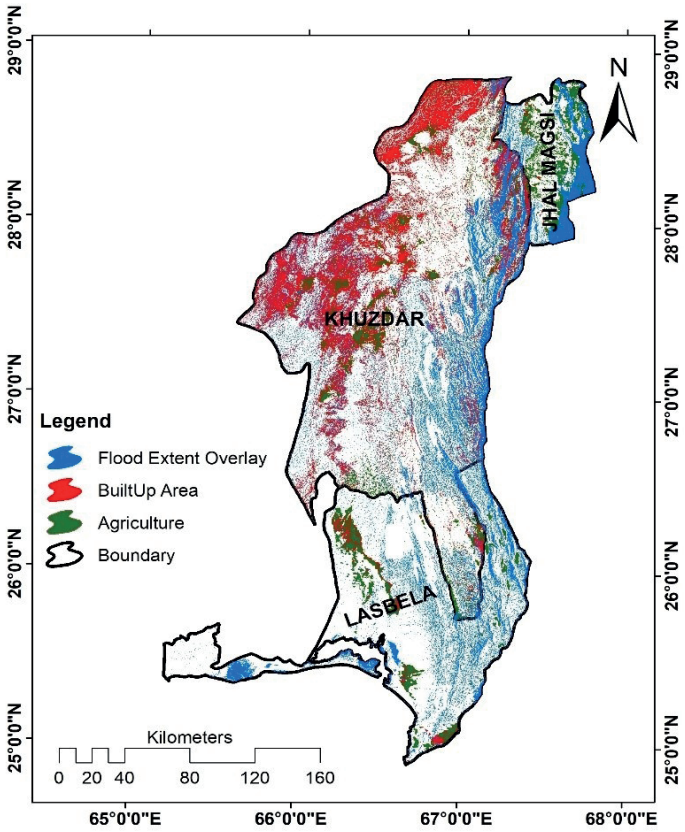


Figure 14. Map showing the flood-effected built-up area and Agricultural land of the Baluchistan Province, Pakistan.

on the day of the flood event show the first signs of the waters beginning to leave the floodplain (Figure 15). Floodwater on September 1st left behind a dense layer of muddy soil that persisted for a while.

The image obtained on September 1st shows the height of the inundation, and the water continued to rise until September 20th. On November 24th, it seems as though things are back to normal. Clarifying the existence and nature of surface changes seen both within and outside of agricultural areas is another benefit of the spectral analysis. Sentinel-2 photos under close examination show distinct patterns of change in nine districts across Punjab, Baluchistan, and Sindh province since August 12. Soon after the floodplain was flooded, all provinces mentioned were submerged under water, and their spectral reflections assumed the typical form of vegetation (Figure 16).

4. Discussion

4.1. Flood Extent Mapping with GEE and SAR Data

The study analyzed recent floods in Punjab, Sindh, and Baluchistan, using Sentinel-1A SAR data on GEE in the districts, Muzaffargarh, Rajanpur, DG Khan, Sanghar, Khairpur, Sukkur, Jhal Magsi, Khuzdar, and Lasbela during August and September 2022. Using a change detection technique, one "pre-flood map"

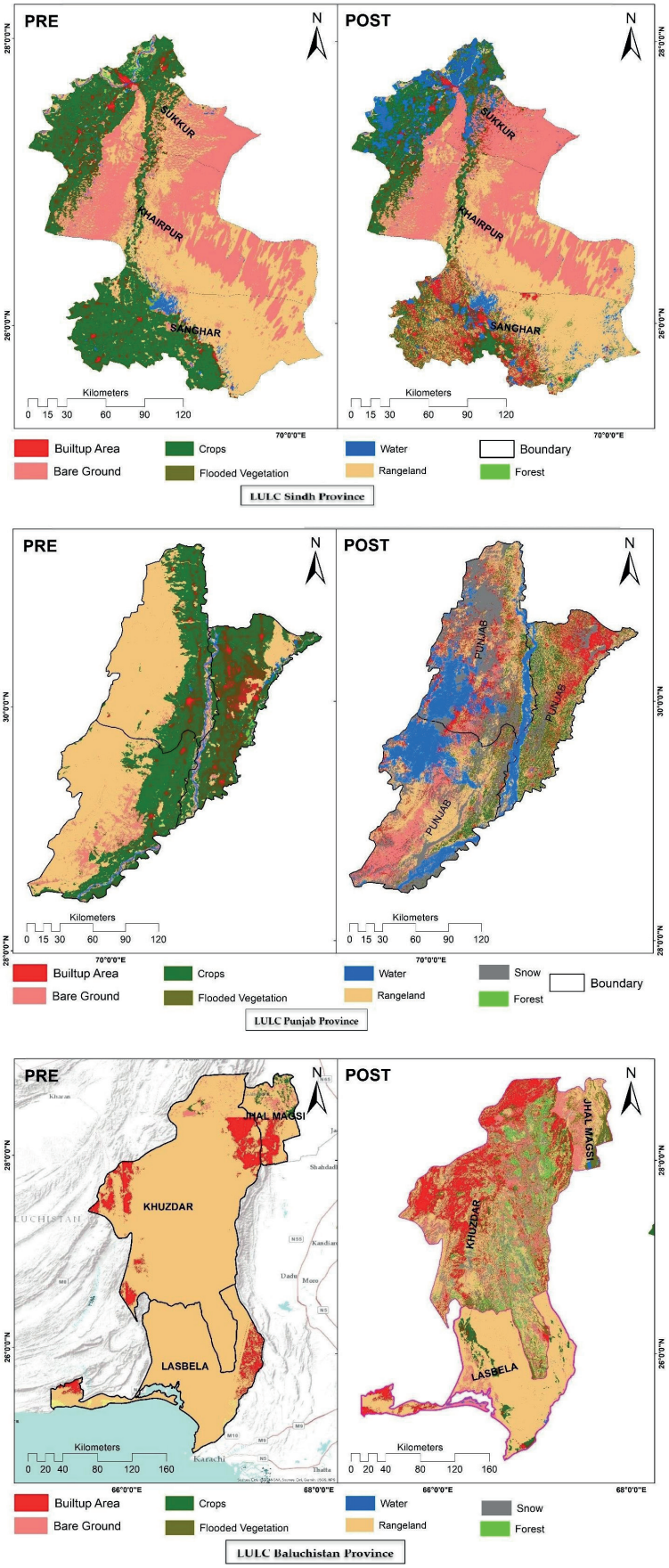


Figure 15. Maps showing the temporal Land Use Land Cover of the Sindh, Punjab and Baluchistan Provinces.

Table 5. Land use land cover types and their total area in the selected regions of study.

Landcover	Area-Km^2	Percentage
Water	17947.18	1.22
Forest	36831.13	2.50
Flooded Vegetation	858.48	0.06
Crops	198411.69	13.48
Built-up Area	42304.25	2.87
Bare Ground	30figure 192.74	20.50
Snow	58880.09	4.00
Rangeland	814340.54	55.35
Total	1471266.11	100

Table 6. The temporal land cover types for the Province of Baluchistan.

	Districts	Landcover Pre-Flood Area		Landcover post-flood Area	
		Classes	Km^2	Classes	Km^2
Temporal Landcover Province Baluchistan	Jhal Magsi	Water	3	Water	64.02
		Crops	835	Crops	320
		Built-up	18	Built-up	120
		Bare Ground	561	Bare Ground	1245
		Rangeland	2435	Rangeland	4700
	Khuzdar	Water	4		
		Crops	617		
		Built-up	91		
		Bare Ground	1096		
		Rangeland	27018		
	Lasbela	Water	138		
		Forest	2		
		Flooded Vegetation	4		
		Crops	779		
		Built-up	102		
		Bare Ground	790		
		Rangeland	10893		

and one "post-flood map" are compared to handle the splitting of water areas. Pre-to-post differences comparison yields a grayscale image that represents change and is made up of single-band continuous data (Ghouri *et al.*, 2024). Whereas darker areas correspond to decreased reflectance, which represents areas covered by water, brighter spots correspond to increased reflectance, which shows the areas not covered by water (Psomiadis *et al.*, 2020 and Gupta *et al.*, 2019).

4.1.1. Sindh Province

The affected agriculture and crop land is 2,365.7 km^2 while the built-up area is 609.8 km^2. The total research area's composite region under flood inundation from August to September was estimated to be 45,727.6 km^2. Using Synthetic Aperture Radar (SAR) images from Sentinel-1A SAR images, the pre-image and pose-image events were used to map the extent of flooding in Sindh province. Along with maps showing how floods affected the agricultural land in the districts of Khairpur, Sanghar, and Sukkur, detailed and compiled flood maps were also created for efficient visualization and hotspot identification. A visual comparison of the flood extent map indicated three distinct regions; Figure 17 illustrates how flood-inundated water severely damaged Sindh province. Floodwaters encompass 497.1 km^2, 565.2 km^2 for the Sanghar district, and 979.9 km^2 for the Khairpur district (Tables 2 and 8). Also, 915.9 km^2 of the cropland area in the Sindh province was flooded, as shown in Figure 12. The backscatter in flooded regions or water bodies is substantially lower than that from other non-water areas attributed to the specular reflectance of C-band signals; this allows the flooded area to be quickly extracted from the SAR images (Chini *et al.*, 2021 and Patra *et al.*, 2011).

Table 7. The temporal land cover types for the Province of Punjab

	Districts	Landcover Pre-Flood Area		Landcover post-flood Area	
		Classes	**Km²**	**Classes**	**Km²**
Temporal Landcover Province Punjab	**D.G Khan**	Water Forest Crops Built-up Bare Ground Rangeland	167 3 3936 383 238 7003	Water Cloud Cover Crops Built-up Bare Ground Rangeland	433 5395 276 1561 905 2698
	Muzaffargarh	Water Forest Crops Built-up Bare Ground Rangeland	343 61 4718 1157 237 1098	Water Cloud Cover Crops Built-up Bare Ground Rangeland	464 1512 1163 1428 132 2138
	Rajanpur	Water Forest Crops Built-up Bare Ground Rangeland	166 7 3893 212 1118 7028	Water Cloud Cover Crops Built-up Bare Ground Rangeland	464 3947 359 891 2188 4099

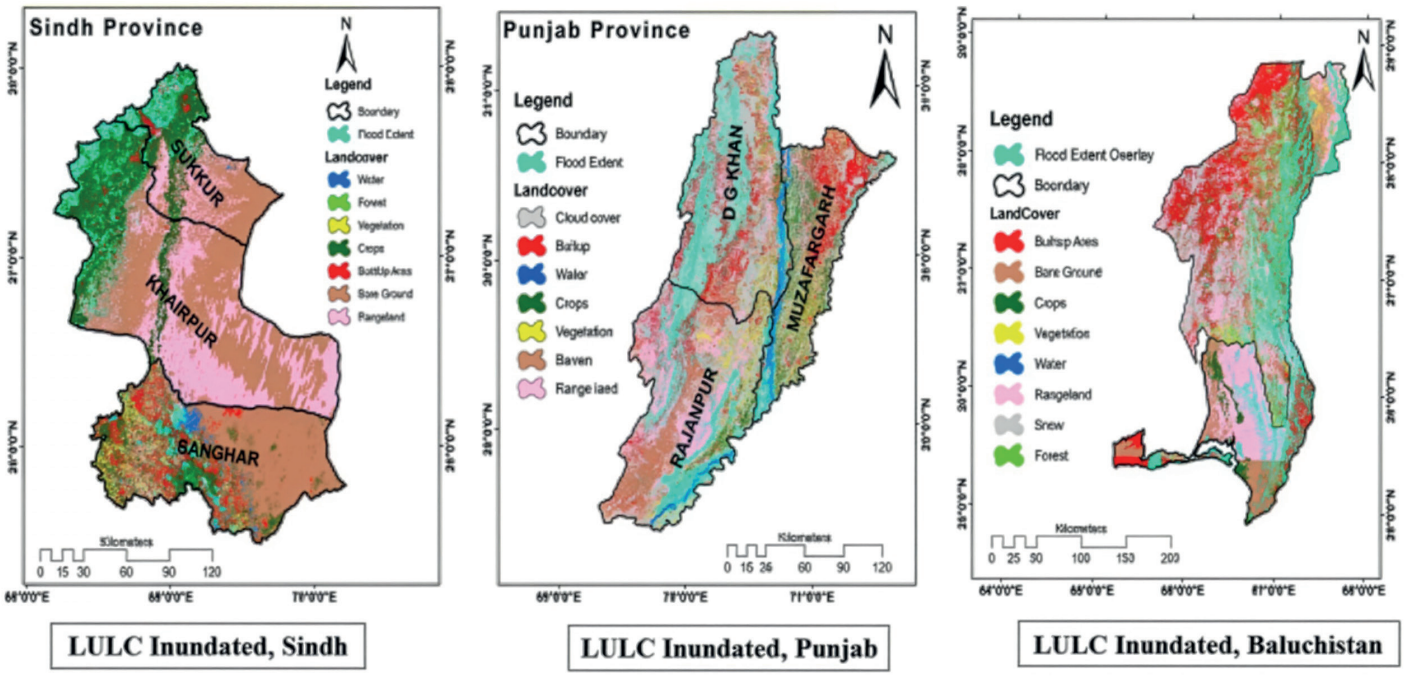


Figure 16. The flood inundated land cover maps of the Sindh, Punjab & Baluchistan provinces.

Table 8. The Flood Extent of the Baluchistan Province.

Flood Extent Map Area Province Sindh	Area	
	Km²	%
Khairpur	979.80	47.98
Sanghar	565.20	27.68
Sukkur	497.09	24.34
Total	2042.09	100

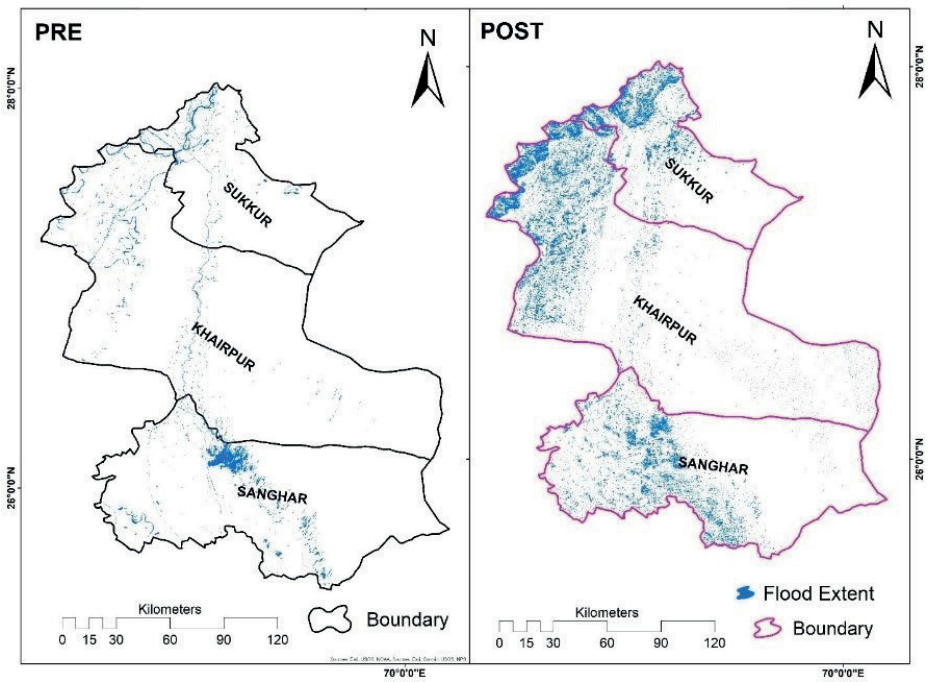


Figure 17. Map showing the pre and post flood extent of the Sindh Province, Pakistan.

4.1.2. Baluchistan Province

In Baluchistan, affected crops and agricultural land cover 674.7 km², compared to the built-up area of 47.8 km². The overall area vulnerable to flood inundation was estimated to be 10,733.4 km² (Figure 18). The situation worsened because of the intense rain in the affected districts (Nanditha *et al.*, 2023). 1,002.2 km² of the Jhal Magsi district, 7,266.5 km² of the Khuzdar district, and 2,464.6 km² of the Lasbela district were submerged by floodwater (Tables 4 & 9).

4.1.3: Punjab Province

Punjab province is characterized by its extensive river systems, including the Indus, Jehlum, Chenab, and Ravi rivers, which make the region prone to both riverine and flash floods (Siddiqui *et al.*, 2018). The river flooding affected a broad region, having a substantial impact on communities, structures, and agriculture/cropland (Qamer *et al.*, 2023 and Ashraf *et al.*, 2023). The built-up area is 297.5 km², while the affected agricultural and cropland is 776.9 km². For the entire research region, the total area subject to flood inundation was calculated to be 4,001.3 km² (Figure 19). Maps show how floods affected the agriculture in the districts of DG Khan, Muzaffargarh, and Rajanpur. Nearly one-third (4,001.3 km²) of the province's total land area was underwater due to flooding brought on by rain. At the district level, DG Khan, Muzaffargarh, and Rajanpur were found to be significantly devastated, with the flooded area marking up around one-fourth of each district (Tables 3 and 10). The areas of the districts that were inundated by the floodwater are 1,871.3 Km² for DG Khan district and 620 km² for Muzaffargarh district while for Rajanpur, it is 1,509.72 km².

South Asia's temperature trends have been rising (Fu *et al.*, 2024). Changes have been made to the patterns of monsoon precipitation, particularly in Punjab, Sindh, and Baluchistan (Qureshi *et al.*, 2023). Regional Climate Model (RCM) indicates that there

Table 9. The Flood Extent of the Baluchistan Province

Flood Extent Map Area Province Baluchistan	Area	
	Km²	%
Jhal Magsi	1002.22	9.34
Khuzdar	7266.54	67.70
Lasbela	2464.66	22.96
Total	10733.42	100

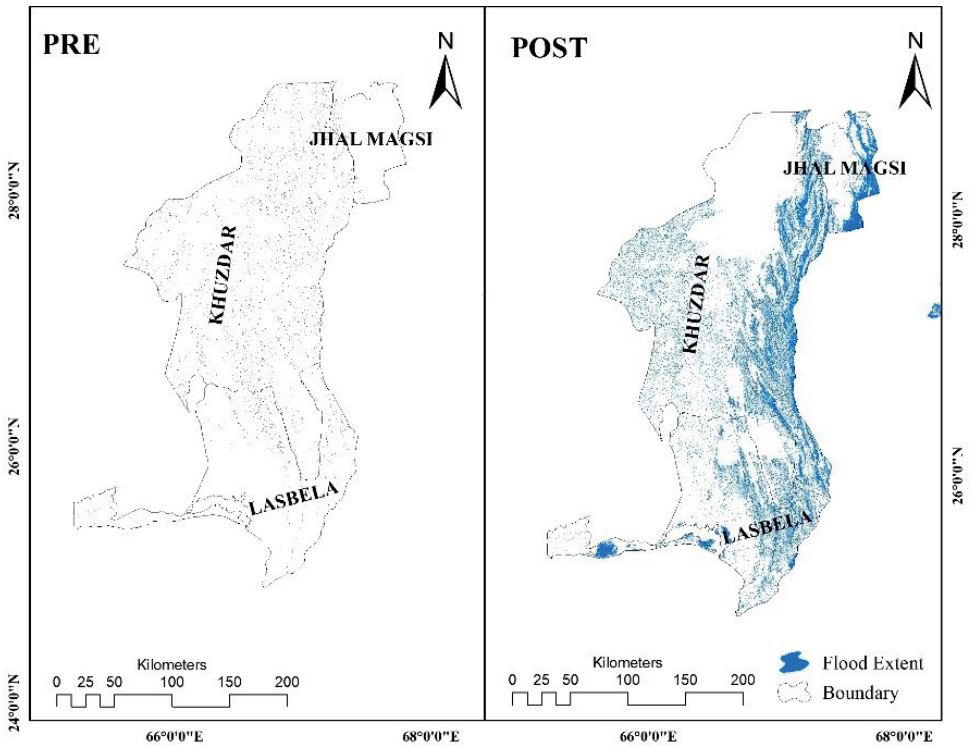


Figure 18. Map showing the flood Extent of the Baluchistan Province, Pakistan.

may be a higher risk of flooding during the monsoon season (Aqib *et al.*, 2024 and Jane *et al.*, 2018). Remotely accessible data is helpful for rescue and restoration efforts both before and after the disaster (Roth *et al.*, 2023). When it comes to flood mapping, satellite data can be extremely helpful in determining the extent of flooding and its effects on croplands, urban population growth, and built-up areas (Arshad *et al.*, 2021). With this information, relief efforts can be launched immediately (Amin *et al.*, 2023). Unfortunately, because of the heavy cloud cover during the floods, optical data from satellites were not available for analysis (Tarpanelli *et al.*, 2022). On the other hand, because Sentinel-1A data is available day and night without affecting cloud cover, it is useful for flood monitoring immediately following any flood event (Pletzer *et al.*, 2022). We have calculated the overall inundation during the flood to be roughly ~ 16,758.5 km², based on Sentinel-1A data. The flood map produced by SAR data was verified by comparing it with the NDWI indices of Sentinel-2 optical data. The flood inundation map matched the grayscale images from the SAR data with accuracy (Patra *et al.*, 2011). Therefore, it turned out to be an effective technology that offers near-immediate surveillance and control of flooding situations on any geographical setup (Tariq and van de Geisen, 2012). These findings of the present research will assist in locating flood-prone areas and those that need to be considered to lessen the effects of calamities that happen naturally. Elements at risk were identified to carry out the analysis of the flooding impact assessment. The LULC map, NDVI, NDWI, and NDBI maps are used to identify the elements in danger. The disaster management authority would receive pertinent information from the SAR-derived flood inundation mapping, along with the potential impact on crops, settlements, and population, to enable a prompt damage assessment and efficient relief efforts.

Table 10. The Flood Extent of the Punjab Province.

Flood Extent Map Area Province Punjab	Area	
	Km²	%
D.G Khan	1871.25	46.77
Muzaffargarh	620.03	15.50
Rajanpur	1509.72	37.73
Total	4001	100.00

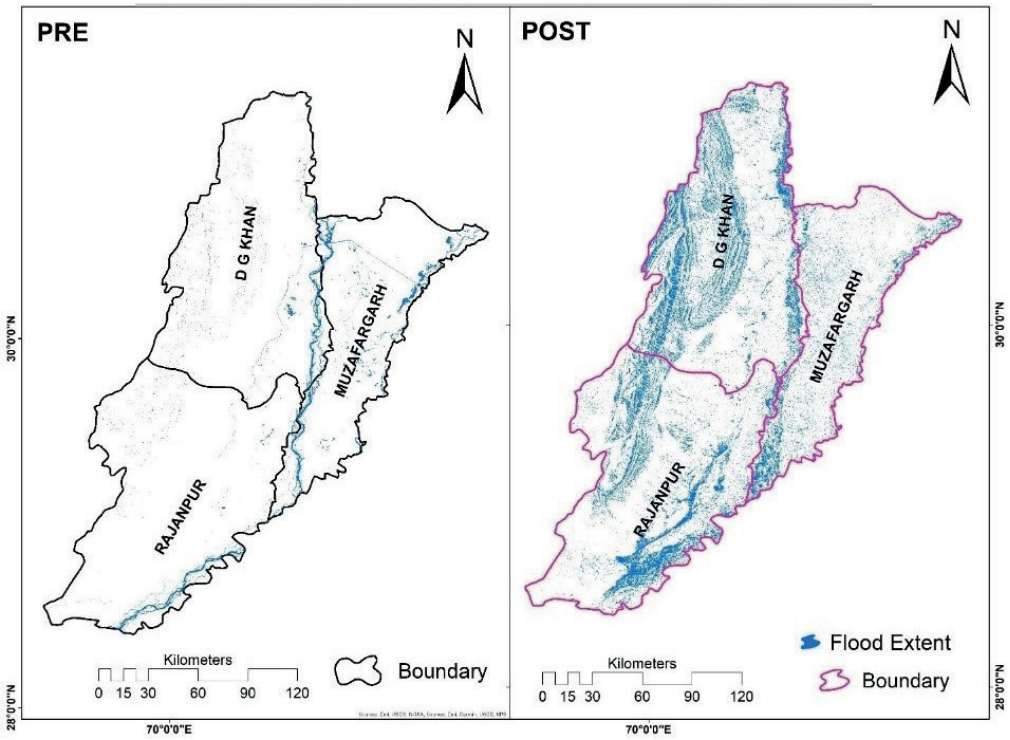


Figure 19. Map showing the pre and post flood extent of the Punjab Province, Pakistan.

5. Conclusions

The benefits of high-resolution multisource RS imagery for mapping extent were emphasized in this study by showing that well multi-temporal RS data can be used to estimate flood inundation and support the evaluation of flood impact on agricultural areas. The outcomes reveal that sufficient spatial and temporal resolution data from the Sentinel-1 mission can be obtained to produce highly accurate flood maps and improve the ability to map the scale and time frame of each flood precisely, assisting in improved estimation of flood impacts on agricultural areas. The analysis of data also indicated that there is still a very small chance of catching a flood event at its height and tracking its development with high spatial and temporal resolution EO data. Additionally, the multi-temporal optical and radar data provided unique information for mapping LULC, permanent water cover, and inundation floods, all of which are ideal for defining the effects of flood events on local communities' crops. The main conclusions are as follows: riverine floods in the primarily flat downstream areas are caused by high-intensity precipitation in the upstream areas of the Indus River Basin. Inundation of up to 16,758.5 Km² has resulted from the floods in the Indus River Basin, negatively affecting both built-up areas (445.5 Km²) and agricultural land (1,692.2 Km²). GEE was also a useful tool for interpreting crucial flood metrics in a pre- and post-flood disaster environment. It is found that combining GEE with SAR and optical RS data improves our knowledge of flood characteristics, including their extent and effects on populated areas and agricultural land. Databases of flood assessment are crucial, especially in the event of a flood disaster when relief-providing organizations and decision-makers need to allocate resources as efficiently as possible. This study also concluded how important

it is to use modern resources like GEE and Sentinel-1 radar to quickly map and evaluate flood disasters in high-risk areas like the Indus River Basin. Future studies on floods in comparable high-risk regions can benefit greatly from the study's focus on the Indus River Basin.

6. References

Ahmad, D., Kanwal, M. and Afzal, M. (2023). Climate change effects on riverbank erosion Bait community flood-prone area of Punjab, Pakistan: an application of livelihood vulnerability index. *Environment, Development and Sustainability*, 25, 9387–9415. doi: **https://doi.org/10.1007/s10668-022-02440-1**

Ali, S., Liu, Y., Ishaq, M., Shah, T., Abdullah, Ilyas, A. and Din, I. (2017). Climate Change and Its Impact on the Yield of Major Food Crops: Evidence from Pakistan. *Foods*, 6(6), 39. doi: **https://doi.org/10.3390/foods6060039**

Amin, F., Luxmi, S., Ali, F., & Fareeduddin, M. (2023). Flood 2022 in Pakistan: Managing medical flood relief camps in a developing country. Journal of Family Medicine and Primary Care, 12(2), 194–200. doi: **https://doi.org/10.4103/jfmpc.jfmpc_1919_22**

Aqib, S., Seraj, M., Ozdeser, H., Khalid, S., Haseeb Raza, M., Ahmad, T. (2024). Assessing adaptive capacity of climate-vulnerable farming communities in flood-prone areas: Insights from a household survey in South Punjab, Pakistan. Climate Services, 33, 100444. doi: **https://doi.org/10.1016/j.cliser.2023.100444**

Arshad, M., Ma, X., Yin, J., Ullah, W., Liu, M. and Ullah, I. (2021). Performance evaluation of ERA-5, JRA-55, MERRA-2, and CFS-2 reanalysis datasets, over diverse climate regions of Pakistan. *Weather and Climate Extremes*, 33, 100373. doi: **https://doi.org/10.1016/j.wace.2021.100373**

Ashraf, I., Ahmad, S. R., Ashraf, U. and Khan, M. (2023). Community perspectives to improve flood management and socio-economic impacts of floods at Central Indus River, Pakistan. *International Journal of Disaster Risk Reduction*, 92, 103718. doi: **https://doi.org/10.1016/j.ijdrr.2023.103718**

Asim, M., Nadeem, M. and Saima, G. (2021). Empowering Communities to cope Flood Risk: Learning from Flood affected Community in Narowal District, Pakistan. *Disaster Advances*, 14(9), 23–33. doi: **https://doi.org/10.25303/149da2333**.

Bai, Y., Wu, W., Yang, Z., Yu, J., Zhao, B., Liu, X., Yang, H., Mas, E. and Koshimura, S. (2021). Enhancement of Detecting Permanent Water and Temporary Water in Flood Disasters by Fusing Sentinel-1 and Sentinel-2 Imagery Using Deep Learning Algorithms: Demonstration of Sen1Floods11 Benchmark Datasets. *Remote Sensing*, 13(11), 2220. doi: **https://doi.org/10.3390/rs13112220**

Carreño Conde, F. and De Mata Muñoz, M. (2019). Flood Monitoring Based on the Study of Sentinel-1 SAR Images: The Ebro River Case Study. *Water*, 11(12), 2454. **doi: https://doi.org/10.3390/w11122454**

Chan, E. Y. Y., Man, A. Y. T. and Lam, H. C. Y. (2019). Scientific evidence on natural disasters and health emergency and disaster risk management in Asian rural-based area. *British Medical Bulletin*, 129(1), 91–105. doi: **https://doi.org/10.1093/bmb/ldz002**

Chini, M., Pelich, R., Liu, Y., Renaud Hostache, Zhao, J., Concetta Di Mauro and Matgen, P. (2021). Sar-Based Flood Mapping, Where We Are and Future Challenges. *2021 IEEE International Geoscience and Remote Sensing Symposium IGARSS, Brussels, Belgium*. **https://doi.org/10.1109/igarss47720.2021.9554975**

Clement, M. A., Kilsby, C. G. and Moore, P. (2017). Multi-temporal synthetic aperture radar flood mapping using change detection. *Journal of Flood Risk Management*, 11(2), 152–168. doi: **https://doi.org/10.1111/jfr3.12303**

Dube, K., Nhamo, G. and Chikodzi, D. (2021). Flooding trends and their impacts on coastal communities of Western Cape Province, South Africa. *GeoJournal*, 87, 453–468. doi: **https://doi.org/10.1007/s10708-021-10460-z**

Ejeta, L. T. (2018). Community's Emergency Preparedness for Flood Hazards in Dire-dawa Town, Ethiopia: A Qualitative Study. *PLoS Currents*, 10. doi: **https://doi.org/10.1371/currents.dis.3843ad9fc823c8c853970148b350750c**

Fankhauser, S. and McDermott, T. K. J. (2014). Understanding the adaptation deficit: Why are poor countries more vulnerable to climate events than rich countries? *Global Environmental Change*, 27, 9–18. doi: **https://doi.org/10.1016/j.gloenvcha.2014.04.014**

Fu, Z.-H., Zhou, W., Zhou, W., Xie, S.-P., Zhang, R. and Wang, X. (2024). Dynamic pathway linking Pakistan flooding to East Asian heatwaves. *Science advances*, 10(17). doi: **https://doi.org/10.1126/sciadv.adk9250**

Gan, T. Y., Zunic, F., Kuo, C.-C. and Strobl, T. (2012). Flood mapping of Danube River at Romania using single and multi-date ERS2-SAR images. *International Journal of Applied Earth Observation and Geoinformation*, 18, 69–81. doi: **https://doi.org/10.1016/j.jag.2012.01.012**

Gao, B. C. (1996). NDWI—A normalized difference water index for remote sensing of vegetation liquid water from space. *Remote Sensing of Environment, 58*(3), 257–266. doi: **https://doi.org/10.1016/S0034-4257(96)00067-3**

Ghouri, A. Y., Rehman, A. ur, Rasheed, F., Miandad, M. and Rehman, G. (2024). Flood Mapping Using the Sentinel-1 SAR Dataset and Application of the Change Detection Approach Technique (CDAT) to the Google Earth Engine In Sindh Province, Pakistan. *Ecological Questions*, 35(2), 1–18. doi: **https://doi.org/10.12775/EQ.2024.024**

Gupta, N., Mathew, A. and Khandelwal, S. (2019). Analysis of cooling effect of water bodies on land surface temperature in nearby region: A case study of Ahmedabad and Chandigarh cities in India. *The Egyptian Journal of Remote Sensing and Space Science*, 22(1), 81–93. doi: **https://doi.org/10.1016/j.ejrs.2018.03.007**

Haque, M. A., Yamamoto, S. S., Malik, A. A. and Sauerborn, R. (2012). Households' perception of climate change and human health risks: A community perspective. *Environmental Health*, 11(1). doi: **https://**

doi.org/10.1186/1476-069x-11-1

Hoang, L. P., Biesbroek, R., Tri, V. P. D., Kummu, M., van Vliet, M. T. H., Leemans, R., Kabat, P. and Ludwig, F. (2018). Managing flood risks in the Mekong Delta: How to address emerging challenges under climate change and socioeconomic developments. *Ambio*, 47(6), 635–649. doi: **https://doi.org/10.1007/s13280-017-1009-4**

Jane, R. A., Simmonds, D. J., Gouldby, B. P., Simm, J. D., Dalla Valle, L. and Raby, A. C. (2018). Exploring the Potential for Multivariate Fragility Representations to Alter Flood Risk Estimates. *Risk Analysis*, 38(9), 1847–1870. doi: **https://doi.org/10.1111/risa.13007**

Joyce, K., Belliss, S., Samsonov, S., McNeill, S. and Glassey, P. (2009). A review of the status of satellite remote sensing and image processing techniques for mapping natural hazards and disasters. *Semantic Scholar*, 33(2). doi: **https://doi.org/10.1177/0309133309339563**

Khan, I., Lei, H., Shah, A. A., Khan, I. and Muhammad, I. (2021). Climate change impact assessment, flood management, and mitigation strategies in Pakistan for sustainable future. *Environmental Science and Pollution Research*, 28(23). doi: **https://doi.org/10.1007/s11356-021-12801-4**

Kirsch, T. D., Wadhwani, C., Sauer, L., Doocy, S. and Catlett, C. (2012). Impact of the 2010 Pakistan Floods on Rural and Urban Populations at Six Months. *PLoS Currents*, 1. doi: **https://doi.org/10.1371/4fdfb212d2432**

Manzoor, Z., Ehsan, M., Khan, M. B., Manzoor, A., Akhter, M. M., Sohail, M. T., Hussain, A., Shafi, A., Abu-Alam, T. and Abioui, M. (2022). Floods and flood management and its socio-economic impact on Pakistan: A review of the empirical literature. *Frontiers in Environmental Science*, 10(10). doi: **https://doi.org/10.3389/fenvs.2022.1021862**

Mbah, M. F., Shingruf, A. and Molthan-Hill, P. (2022). Policies and practices of climate change education in South Asia: towards a support framework for an impactful climate change adaptation. *Climate Action*, 1(1). doi: **https://doi.org/10.1007/s44168-022-00028-z**

Nanditha, J. S., Kushwaha, A. P., Singh, R., Malik, I., Solanki, H., Chuphal, D. S., Dangar, S., Mahto, S. S., Vegad, U. and Mishra, V. (2023). The Pakistan Flood of August 2022: Causes and Implications. *Earth's Future*, 11(3). doi: **https://doi.org/10.1029/2022ef003230**

Otto, Zachariah, M., Saeed, F., Siddiqi, A., Kamil, S., Mushtaq, H., Arulalan T, AchutaRao, K., T, C. S., Barnes, C., Philip, S., Kew, S. F., Vautard, R., Koren, G., Pinto, I., Wolski, P., Maja Vahlberg, Singh, R., Arrighi, J. and Maarten van Aalst (2023). Climate change increased extreme monsoon rainfall, flooding highly vulnerable communities in Pakistan. *Environmental Research: Climate*, 2(2), 025001–025001. doi: **https://doi.org/10.1088/2752-5295/acbfd5**

P Lama, A., & Tatu, U. (2022). Climate change and infections: lessons learnt from recent floods in Pakistan. *New microbes and new infections*, 49-50, 101052. doi: **https://doi.org/10.1016/j.nmni.2022.101052**

Patra, S., Ghosh, S. and Ghosh, A. (2011). Histogram thresholding for unsupervised change detection of remote sensing images. *International Journal of Remote Sensing*, 32(21), 6071–6089. doi: **https://doi.org/10.1080/01431161.2010.507793**

Pletzer, J. F., Hauglustaine, D., Cohen, Y., Jöckel, P. and Grewe, V. (2022). The Climate Impact of Hypersonic Transport. *The Climate Impact of Hypersonic Transport, EGUsphere*. doi: **https://doi.org/10.5194/egusphere-2022-285**

Psomiadis, E., Diakakis, M. and Soulis, K. X. (2020). Combining SAR and Optical Earth Observation with Hydraulic Simulation for Flood Mapping and Impact Assessment. *Remote Sensing*, 12(23), 3980. doi: **https://doi.org/10.3390/rs12233980**

Qamer, F. M., Abbas, S., Ahmad, B., Hussain, A., Salman, A., Muhammad, S., Nawaz, M., Shrestha, S., Iqbal, B. and Thapa, S. (2023). A framework for multi-sensor satellite data to evaluate crop production losses: the case study of 2022 Pakistan floods. *Scientific Reports*, 13(1), 4240. doi: **https://doi.org/10.1038/s41598-023-30347-y**

Quintero, F., Sempere-Torres, D., Berenguer, M. and Baltas, E. (2012). A scenario-incorporating analysis of the propagation of uncertainty to flash flood simulations. *Journal of Hydrology*, 460-461, 90–102. doi: **https://doi.org/10.1016/j.jhydrol.2012.06.045**

Qureshi, H., Syed and Fang Yenn Teo (2023). Trend assessment of changing climate patterns over the major agro-climatic zones of Sindh and Punjab. *Frontiers in water*, 5. doi: **https://doi.org/10.3389/frwa.2023.1194540**

Rana, V. K. and Suryanarayana, T. M. V. (2021). Estimation of flood influencing characteristics of watershed and their impact on flooding in data-scarce region. *Annals of GIS*, 1–22. doi: **https://doi.org/10.1080/19475683.2021.1960603**

Roth, F., Bauer-Marschallinger, B., Tupas, M. E., Reimer, C., Salamon, P. and Wagner, W. (2023). Sentinel-1-based analysis of the severe flood over Pakistan 2022. *Natural Hazards and Earth System Sciences*, 23(10), 3305–3317. doi: **https://doi.org/10.5194/nhess-23-3305-2023**

Schumann, G., Giustarini, L., Tarpanelli, A., Jarihani, B. and Martinis, S. (2022). Flood Modeling and Prediction Using Earth Observation Data. *Surveys in Geophysics*, 44, 1553-1578. doi: **https://doi.org/10.1007/s10712-022-09751-y**

Shah, A. H., Shahid, M., Tahir, M., Natasha, N., Bibi, I., Tariq, T. Z., Khalid, S., Nadeem, M., Abbas, G., Saeed, M. F., Ansar, S. and Dumat, C. (2023). Risk assessment of trace element accumulation in soil and Brassica oleracea after wastewater irrigation. *Environmental Geochemistry and Health*, 45(12), 8929–8942. doi: **https://doi.org/10.1007/s10653-022-01351-4**

Siddiqui, M. J., Haider, S., Gabriel, H. F. and Shahzad, A. (2018). Rainfall–runoff, flood inundation and sensitivity analysis of the 2014 Pakistan flood in the Jhelum and Chenab river basin. *Hydrological Sciences Journal*, 63(13-14), 1976–1997. doi: **https://doi.org/10.1080/02626667.2018.1546049**

Tariq, M.A.U.R. and van de Giesen, N. (2012). Floods and flood management in Pakistan. *Physics and Chemistry of the Earth, Parts A/B/C*, 47-48, 11–20. **https://doi.org/10.1016/j.pce.2011.08.014**

Tarpanelli, A., Mondini, A. C. and Camici, S. (2022). Effectiveness of Sentinel-1 and Sentinel-2 for flood detection assessment in Europe.

Natural Hazards and Earth System Sciences, 22(8), 2473–2489. doi: **https://doi.org/10.5194/nhess-22-2473-2022**

Ting, M., Michela Biasutti and You, Y. (2023). Climate warming contributes to the record-shattering 2022 Pakistan rainfall. *Research Square (Research Square)*. doi: **https://doi.org/10.21203/rs.3.rs-2925453/v1**

Try, S., Tanaka, S., Tanaka, K., Sayama, T., Hu, M., Sok, T. and Oeurng, C. (2020). Projection of extreme flood inundation in the Mekong River basin under 4K increasing scenario using large ensemble climate data. *Hydrological Processes*, 34(22), 4350–4364. doi: **https://doi.org/10.1002/hyp.13859**

Wang, L. (2022). A review of the flood management: from flood control to flood resilience. *Heliyon*. *8*(11). doi: **https://doi.org/10.1016/j.heliyon.2022.e11763**

Zha, Y., Gao, J., & Ni, S. (2003). Use of normalized difference built-up index in automatically mapping urban areas from TM imagery. *International Journal of Remote Sensing, 24*(3), 583–594. doi: **https://doi.org/10.1080/01431160304987**

Zhao, J., Chen, H., Liang, Q., Xia, X., Xu, J., Hoey, T., Barrett, B., Renaud, F.G., Bosher, L. and Zhou, X. (2021). Large-scale flood risk assessment under different development strategies: the Luanhe River Basin in China. *Sustainability Science*, 17, 1365–1384. doi: **https://doi.org/10.1007/s11625-021-01034-6**